Supporting Information for "Quasi-2-day wave in low-latitude atmospheric winds as viewed from the ground and space during January-March, 2020"

Maosheng He[1], Jorge L. Chau[1], Jeffrey M. Forbes[2], Xiaoli Zhang[2], Christoph

R. Englert[3], Brian J. Harding[4], Thomas J. Immel[4], Lourivaldo M. Lima[5], S.

Vijaya Bhaskar Rao[6], M. Venkat Ratnam[7], Guozhu Li[8,9], John M.

Harlander[10], Kenneth D. Marr[3], Jonathan J. Makela[11]

[1]Leibniz-Institute of Atmospheric Physics at the Rostock University, Kühlungsborn, Germany.

[2]Ann & H.J. Smead Department of Aerospace Engineering Sciences, University of Colorado, Boulder, USA.

[3]Space Science Division, Naval Research Laboratory, Washington, DC.

[4]Space Sciences Laboratory, University of California Berkeley, Berkeley, CA.

[5]Universidade Estadual da Paraíba, Brazil.

[6]Department of Physics, Sri Venkateswara University, Tirupati, India.

[7]National Atmospheric Research Laboratory, Tirupati, India.

[8]Beijing national observatory of space environment, Institute of Geology and Geophysics, Chinese Academy of Sciences, Beijing, China.

[9]College of Earth and Planetary Sciences, University of Chinese Academy of Sciences, Beijing, China.

[10]Space Systems Research Corporation, Alexandria, VA.

[11]Department of Electrical and Computer Engineering, University of Illinois at Urbana-Champaign, Urbana, IL.

March 19, 2021, 10:27am

Contents of this file

1. Figures S1 to S3

Additional Supporting Information (Files uploaded separately)

1. Captions for Figures S1 to S3

Introduction

The current supporting information comprises three figures.

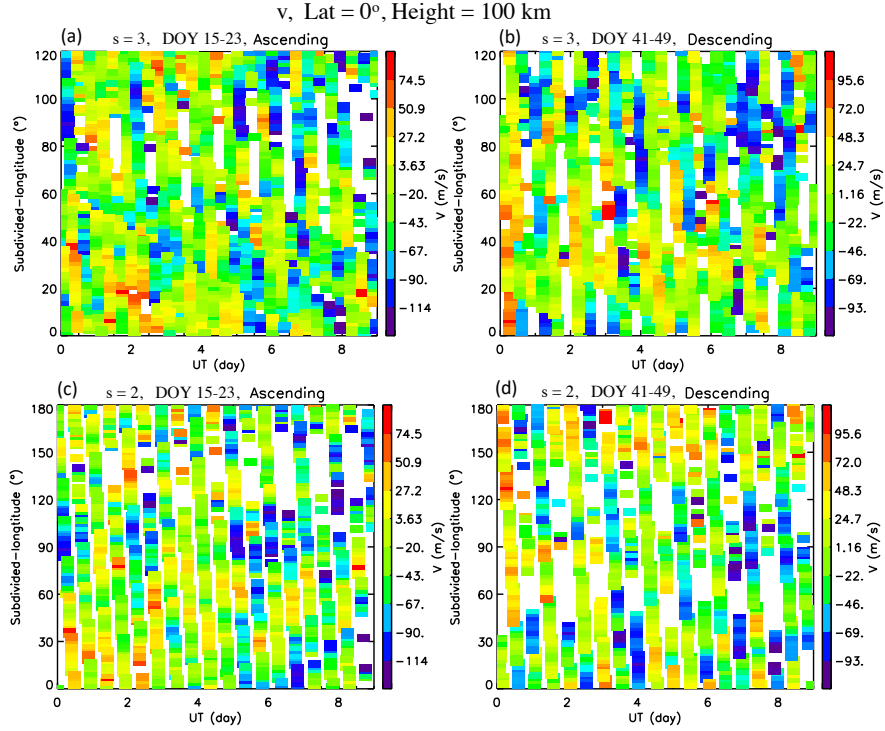———————

v, Lat = 0°, Height = 100 km

Figure S1. MIGHTI meridional wind at 100 km altitude between 5°S–5°N as a function of subdivided longitude and time for estimating the Q2DW+3 amplitude during DoY (a) 15–23 and (b) 41–49 collected on the ascending and descending legs. (c,d) same plots as (a,b) but for the Q2DW+2 amplitude estimation. Outliers outside ± 100 ms^{-1} of the median value have been removed. The sampling distributions here are broadly representative of all the fits that were performed, although the details differ slightly between all latitudes and altitudes and sampling intervals. The subdivided longitude was defined so that $\lambda'(s) := \lambda - 2\pi N_s/s$, $N_s \in \{0, 1, ..., s-1\}$, and $0 < \lambda'(s) < 2\pi/s$, (cf, "longitude subdivision method", LSM, in Moudden & Forbes, 2014). The LSM provides an adequate representation for inspecting the data coverage. At a given latitude, ICON's ascending or descending leg crosses a given longitudinal sector λ once per day and crosses the $\lambda'(s)$ sectors s times per day or $\frac{sT}{1\text{day}}$ times per wave period T (i.e., 6 and 4 times per 48hr for Q2DW+3 and Q2DW+2 as demonstrated in (a, b) and (c, d), respectively).
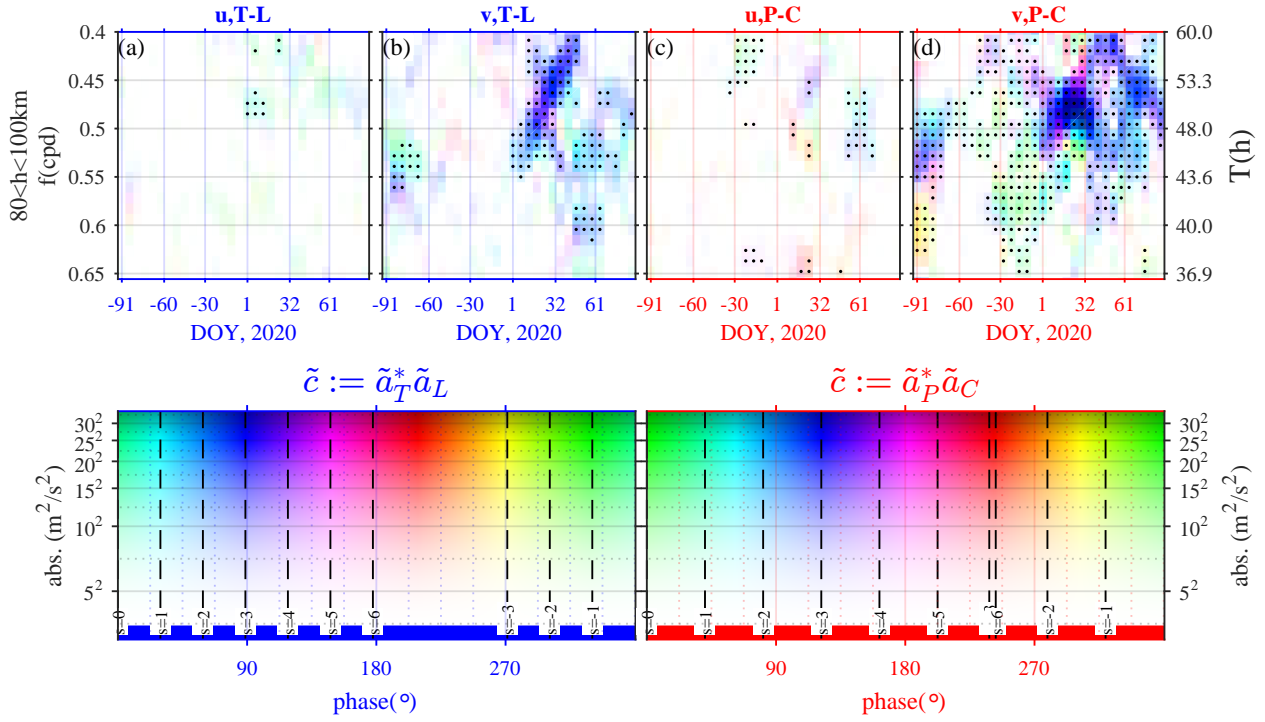
March 19, 2021, 10:27am

Figure S2. (a) Altitude-averaged (80–100 km) cross product between the 23-day sliding Lomb-Scargle spectrum of the zonal wind collected by the radar at Tirupati and that at Ledong . (b) Same as (a) but for the meridional wind. (c,d) same as (a,b) but between at the Peru-Cariri radar pair. In each panel, the darkness denotes the magnitude; the color hue denotes the longitudinal phase difference which enables determining the zonal wavenumber refers to the color map; and the black dots indicate spectra above the $\alpha = 0.01$ significance level (for details cf, He et al., 2018; He, Chau, et al., 2020). The color bar for each pair are indicated in the bottom row.
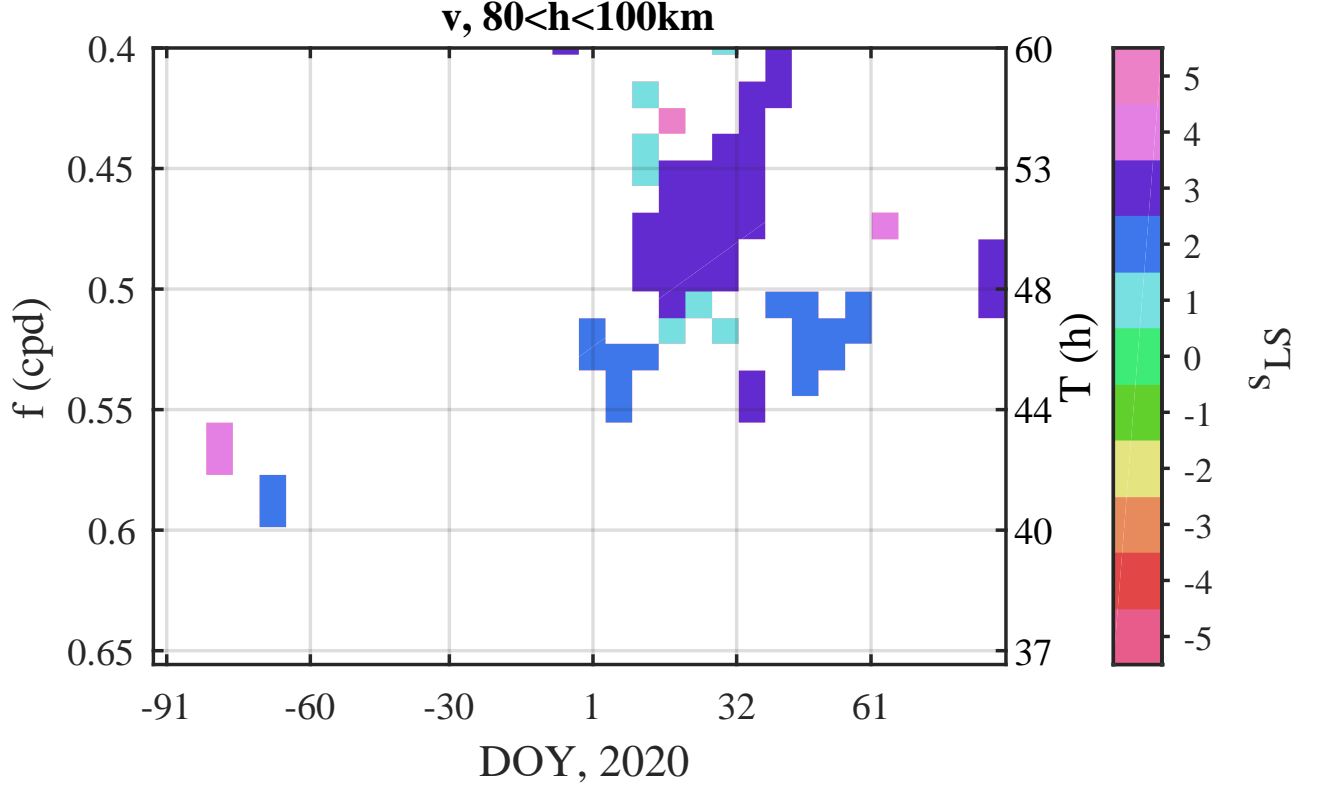
Figure S3. The dominant zonal wavenumber at 80–100km altitude estimated using the meridional winds from all four stations through the least square method $\hat{s}_{LS} = \text{argmin}_{s \in \{-5,-4,...,5\}} \sum_k |\tilde{a}_k - \tilde{A}_0(s)e^{is\lambda_k}|^2$ (see Equation A3 He, Forbes, et al., 2020, for details). Here, $\hat{s}_{LS}$ is displayed only when the least-square coefficient of determination $r^2 > 0.7$ and the Lomb-Scargle spectra $\tilde{a}_k$ are above the significance level $\alpha = 0.01$ at all four stations.

References

He, M., Chau, J. L., Forbes, J. M., Thorsen, D., Li, G., Siddiqui, T. A., . . . Hocking, W. K. (2020). Quasi-10-Day Wave and Semidiurnal Tide Nonlinear Interactions During the Southern Hemispheric SSW 2019 Observed in the Northern Hemispheric Mesosphere. *Geophys. Res. Lett.*, *47*(23), e2020GL091453. Retrieved from `https://doi.org/10.1029/2020GL091453` doi: https://doi.org/10.1029/2020GL091453

He, M., Chau, J. L., Stober, G., Li, G., Ning, B., & Hoffmann, P. (2018). Relations Between Semidiurnal Tidal Variants Through Diagnosing the Zonal Wavenumber Using a Phase Differencing Technique Based on Two Ground-Based Detectors. *J. Geophys. Res. Atmos.*, *123*(8), 4015–4026. Retrieved from `https://doi.org/10.1002/2018JD028400` doi: 10.1002/2018JD028400

He, M., Forbes, J. M., Chau, J. L., Li, G., Wan, W., & Korotyshkin, D. V. (2020). High-Order Solar Migrating Tides Quench at SSW Onsets. *Geophys. Res. Lett.*, *47*(6), 1–8. Retrieved from `https://doi.org/10.1029/2019GL086778` doi: 10.1029/2019GL086778

Moudden, Y., & Forbes, J. M. (2014). Quasi-two-day wave structure, interannual variability, and tidal interactions during the 2002–2011 decade. *J. Geophys. Res.*, *119*(5), 2241–2260. doi: 10.1002/2013JD020563